RSC Advances




ROYAL SOCIETY OF CHEMISTRY

www.rsc.org/advances

Journal Name

RSCPublishing

ARTICLE

# High Efficiency Photocatalytic Conversion of $CO_2$ with $H_2O$ over Pt/$TiO_2$ Nanoparticles

Cite this: DOI: 10.1039/x0xx00000x

*Yan Wang*[a], *Qinghua Lai*[a], *Fan Zhang*[a,b], *Xiaodong Shen*[c], *Maohong Fan*[a,d]*, *Yiming He*[a,e], *Shenqiang Ren*[f],

Received 00th January 2012,
Accepted 00th January 2012

DOI: 10.1039/x0xx00000x

www.rsc.org/

The objective of this research was to convert $CO_2$ to $CH_4$ using photocatalysis. In this investigation, well-crystallized anatase $TiO_2$ nanoparticles with diameters of ~ 18.4 nm and a BET surface area of 108.3 $m^2/g$ were synthesized by a solvothermal method and then Pt/$TiO_2$ nanocomposites with high photocatalytic performance and stability were prepared by photoreduction. The average diameter of the well-dispersed Pt nanoparticles was 1.82 nm. The optimal $TiO_2$ calcination temperature was 500 °C, while Pt photodeposition time was 1 h. The photoluminescence (PL) spectra demonstrated that the efficiency of photogenerated charge transfer and separation of Pt/$TiO_2$ was better than that of Pt/P25. For the optimized Pt/$TiO_2$ photocatalysts, the $CH_4$ yield reached 60.1 μmol/($g_{cat}$·h), together with a $H_2$ yield of 87.5 μmol/($g_{cat}$·h) and an $C_2H_6$ yield of 2.8 μmol/($g_{cat}$·h) at 4 h of irradiation. The photocatalytic $CO_2$ conversion ability of Pt/$TiO_2$ was 3.7 times that of Pt/P25. Longer irradiation would result in an increase of $H_2$ output, but not the output of $CH_4$ or $C_2H_6$. With 10.0% $CO_2$, the $CH_4$ yield and $H_2$ yield reached 54.4 μmol/($g_{cat}$·h) and 80.2 μmol/($g_{cat}$·h), respectively. $O_2$ was detected and recorded for a systematic analysis of the relationship between $CO_2$ conversion and water splitting. In addition, the photogenerated electron-hole balance was calculated and an associated reaction mechanism was proposed.

## 1. Introduction

The rapid increase in anthropogenic $CO_2$ emissions is of great concern, since fossil fuel consumption is not likely to cease in the foreseeable future,[1-3] and one major $CO_2$ emission source is the flue gas from power plants.[4] Although $CO_2$ capture and storage (CCS) have been suggested, the ability and environmental consequences of storing several billion tons of $CO_2$ per year are uncertain and costly.[5] Another great challenge that has attracted high attention is the depletion of fossil fuels and the subsequent contribution to an energy crisis.[6] One promising strategy for solving both issues is to develop new utilization methods for converting $CO_2$ into useful chemicals and clean fuels, which however is energy-intensive since $CO_2$ is very stable. A potentially cost-effective approach is to harness the nearly limitless energy available in sunlight by using efficient photocatalysts to perform these conversions.[7] If $CO_2$ can be converted into useful products like CO, $CH_4$ or $CH_3OH$ using solar energy, it will serve to reduce atmospheric $CO_2$ concentrations while providing a renewable energy fuel compatible with our current energy infrastructure.[8]

Various attempts have been made at photocatalytic $CO_2$ conversion.[9-11] Among the reported photocatalysts, $TiO_2$ has been investigated most frequently due to its robust reactivity, commercial availability and chemical stability. However, $TiO_2$ still has several disadvantages including the limit to only UV light absorption due to its wide band-gap, and low quantum efficiency resulting from the quick recombination of photogenerated electron-hole pairs.[12-14] To resolve these issues and increase the photocatalytic efficiency of $TiO_2$, great endeavors have been made and they can be generally classified into two kinds. The first way to enhance the photoactivity of $TiO_2$ is through $TiO_2$ modification. Numerous modifications have been made, including metal or nonmetal ions doping, dye sensitization, semiconductor combination and noble metal loading.[15] Noble metal loading refers to the loading of Ag, Au, Pt, Pd, etc. on the surface of $TiO_2$. The loaded noble metal has a higher work function than $TiO_2$, which induces the formation of a Schottky barrier in the $TiO_2$-metal region. Thus, the photogenerated electrons can migrate from $TiO_2$ conduction band (CB) to the metal phase, retarding the recombination of electron-hole pairs and subsequently increasing the photocatalytic activity.[16, 17] Among the noble metal loaded $TiO_2$

photocatalysts, Pt/$TiO_2$ has attracted much attention due to its much higher photoactivity than bare $TiO_2$. For example, Zhang et al. prepared Pt/P25 photocatalyst and used it to convert $CO_2$ to $CH_4$ through photocatalysis, and the $CH_4$ yield was 2.34 μmol/($g_{cat}$·h).[18] Zhai and coworkers also tested the photoactivity of Pt/P25 to convert $CO_2$, and the $CH_4$ yield was 11 μmol/($g_{cat}$·h), which was 9.2 times that of pure P25.[19]

The second way to enhance the photoactivity of $TiO_2$ is to improve the crystallinity and surface area of $TiO_2$, so that the photogenerated charge carriers have better migration and separation ability. $TiO_2$ nanoparticles prepared with high crystallinity and large surface areas are widely utilized in organic decomposition and $H_2$ generation.[20-23] Jiao et al. prepared $TiO_2$ hollow spheres with well-crystallized anatase phase and a large surface area of 104 $m^2$/g to obtain high photocatalytic phenol degradation rates.[24] Yu and coworkers prepared Pt/$TiO_2$ nanosheets with a surface area of 94 $m^2$/g and used them in photocatalytic $H_2$ generation. The photocatalytic $H_2$ generation rates of the Pt/$TiO_2$ nanosheets were 1.5 times higher than that of Pt/P25 ($S_{BET}$=41 $m^2$/g).[25] Nevertheless, the research of photocatalytic $CO_2$ conversion using $TiO_2$ with a large surface area is still scarce, and most research using Pt/$TiO_2$ for photocatalytic $CO_2$ conversion only focuses on P25 with a surface area of around 50 $m^2$/g,[24] which largely limits the improvement of the photocatalytic ability of Pt/$TiO_2$ systems. In order to further improve the photocatalytic $CO_2$ conversion ability of Pt/$TiO_2$ photocatalysts, an effective synthetic method to produce $TiO_2$ with good crystallinity and a large surface area is needed.

The solvothermal method has been gaining continuous interest because of its ease in controlling the size, crystal phase, size distribution and minimizing agglomeration.[15] In this investigation, anatase $TiO_2$ nanoparticles with large surface areas were synthesized by a novel solvothermal method. Pt nanoparticles were deposited on the surface of $TiO_2$ through photoreduction. The influence of $TiO_2$ substrate and Pt deposition time were thoroughly studied. Although $CH_4$, CO and $CH_3OH$ were widely reported as photocatalytic $CO_2$ conversion products, the concentration change with reaction time hasn't been fully investigated. This doesn't facilitate the understanding of the reaction mechanism. 10.0% $CO_2$ with the balance gas of $N_2$ was used to mimic the flue gas and to test the photocatalytic $CO_2$ conversion efficiency as well. Although it is widely accepted that the photocatalytic $CO_2$ conversion is accompanied with water splitting, only reductive products, such as $CH_4$, $CH_3OH$, $H_2$, were reported in many investigations.[8, 26] The lack of $O_2$ might raise questions regarding the reliability of previous experimental data and generate confusion on the relationship of $CO_2$ conversion and water splitting. So in this work, a detailed analysis on $CO_2$ conversion together with water splitting was conducted. The balance of generated electrons and holes was calculated. This might provide some insight into understanding photocatalytic $CO_2$ conversion mechanisms.

## 2. Experimental

### 2.1 Materials preparation and characterization

All chemicals were purchased and directly used without any further purification. $TiO_2$ was prepared by a solvothermal method. First, 0.22 mol $CH_3CH_2OH$ (200 proof, Decon Labs), 0.28 mol $CH_3COOH$ (glacial, Fisher-Scientific) and 0.12 mol deionized (DI) $H_2O$ were mixed to form solution A. Then, 0.35 mol $CH_3CH_2OH$ and 0.04 mol titanium n-butoxide (reagent grade, 97%, Sigma-Aldrich) were mixed to form solution B. Next, solution A was dropped into solution B under stirring to make a homogeneous transparent yellowish sol. The final sol was stirred for 1 h before being introduced into a 200 mL Teflon-lined stainless steel autoclave. The autoclave was maintained at 180 °C for 24 h. $TiO_2$ powder was obtained by centrifuging, washing with ethanol and DI water for several times, and then drying at 80 °C for 24 h. Finally, the materials were heated with a temperature increase rate of 2 °C /min and then calcined at 500 °C for 2 h.

The Pt/$TiO_2$ was prepared by the photoreduction method. First, 0.2 g $TiO_2$ was suspended in a mixture of 30 mL DI $H_2O$, 6 mL 1 mg/mL $H_2PtCl_6$ (8 wt% chloroplatinic acid solution, Sigma-Aldrich) and 10 mL 0.1 mol/L $CH_3OH$ (HPLC grade, Fisher-Scientific). Then, the whole suspension was stirred for 0.5 h before being irradiated with a 500W Xe lamp (Newport) for a certain time. Next, the Pt/$TiO_2$ samples were separated by filtration, washed repeatedly with DI water, and finally dried at 80 °C in a vacuum oven for 24 h. For comparison, Pt/P25 (Degussa) was also prepared by the same procedure.

UV-vis absorption spectra were obtained on a Cary 4000 UV-vis spectrophotometer (Varian), using MgO as reference (99+%, metals basis, Alfa Aesar). Photoluminescence (PL) spectra were measured by a Cary Eclipse fluorescence spectrophotometer (Varian). BET (Brunauer-Emmett-Teller) surface area was measured by a Quantachrome Autosorb IQ automated gas sorption analyzer with an outgas temperature of 180 °C for 3 h and a $N_2$ adsorption-desorption isotherm. Scanning electron microscopy (SEM) images were obtained by an FEI Quanta 450 field emission scanning electron microscope with a Schottky field emission gun at an accelerating voltage of 20 kV. High resolution scanning transmission electron microscopy (HR-STEM) was taken by an FEI Tecnai G2 F20 S-Twin 200 kV transmission electron microscope. X-ray diffraction (XRD) data were collected using a Rigaku Smart Lab automated powder diffraction system. Runs were made with a scan range of 20-80° at 5°/min with a step increment of 0.02°. X-ray photoelectron spectroscopy (XPS) analysis was performed using a Physical Electronics ESCA 5800 spectrometer. High-resolution XPS scans were performed with a pass energy of 23.5 eV and a step size of 0.1 eV. Adventitious carbon was used to determine the induced offset of the binding energy of the C1s peak (284.8 eV) due to surface charging effects. Inductively coupled plasma optical emission spectroscopy (ICP-OES) analysis was tested on a PerkinElmer Optima 8300 ICP-OES spectrometer.

### 2.2 Photocatalytic $CO_2$ conversion experiments

The experimental apparatus built for photocatalytic $CO_2$ conversion is shown in **Fig. 1**. It consists of three parts, including a light source unit, a photocatalytic reaction system, and online product measurement equipment. The photocatalytic $CO_2$ conversion was carried out in a 132 mL stainless steel reactor (4) with an inner Teflon liner and a quartz window on the top of the reactor. A 500W Xe lamp (3b) was used for illumination. A heating tape (8b) with a temperature controller (8c) was used to regulate the reaction temperature when heating was needed. Typically, 0.02 g photocatalyst was placed on a Teflon catalyst holder in the upper region of the reactor and 5 mL DI water was pre-injected into the bottom of the reactor. Before reaction, $CO_2$ was used to purge the system for 1 h to completely remove the air inside the reactor. The pressure of $CO_2$ (laser grade, ~ 21 mmol in total) inside the reactor was regulated to 4 bar. Then the Xe lamp was turned on and the photocatalysts would react with the water vapor and $CO_2$ under illumination. After 4 hours of reaction, the Xe lamp was turned off

and both the gas and liquid components were analyzed. An SRI 8610 C gas chromatograph with two FID detectors and one TCD detector was used to detect the gas component. The columns used were 6' MS-13X, 6' HAYESEP-D and 60M MXT-1. The liquid component was detected by an Agilent Technologies 1260 Infinity high-performance liquid chromatograph (HPLC) with a Refractive Index Detector and Zorbax carbohydrate analysis column and Agilent 5975 C gas chromatography mass spectrometer (GC-MS) with a Triple-Axis Detector and an HP-5MS column.

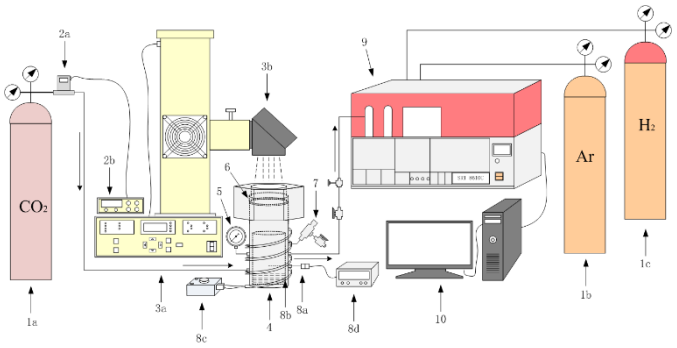


**Fig. 1** Schematic diagram of the photocatalytic $CO_2$ conversion set up. (1a) $CO_2$ (1b) Ar (1c) $H_2$ (2a) mass flow meter (2b) mass flow controller (3a) light intensity controller (3b) light source (4) reactor (5) pressure gauge (6) quartz glass (7) pressure relief valve (8a) thermocouple (8b) heating tape (8c) temperature controller (8d) temperature displayer (9) gas chromatograph (10) computer

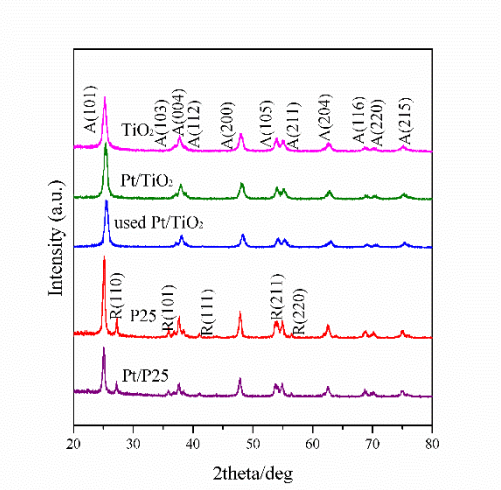


**Fig. 2** XRD patterns of $TiO_2$, Pt/$TiO_2$, used Pt/$TiO_2$, P25 and Pt/P25

## 3. Results and discussions

### 3.1 Characteristics of catalysts

**3.1.1 XRD analysis** The structure of photocatalysts was characterized by XRD. **Fig. 2** shows the XRD patterns of $TiO_2$, Pt/$TiO_2$, used Pt/$TiO_2$, P25 and Pt/P25. It can be observed that the deposition of Pt did not generate any Pt peaks, which might result from the low loading amount of Pt (less than 1% of Pt/$TiO_2$) and the extremely small size of Pt nanoparticles (1-3 nm).[18] Only typical anatase $TiO_2$ diffraction peaks of (101), (103), (004), (112), (200), (105), (211), (204), (116), (220) and (215) were observed for Pt/$TiO_2$ samples. The average crystal size was calculated using Debye-Scherrer equation by peak (101), (004) and (200):

$$D = 0.89\times\lambda/(\beta\cos\theta)$$

where D is the crystal size, λ is the X-ray wavelength (1.54056 Å), β is the full-width at half maximum (FWHM) of the diffraction peak and θ is the diffraction angle.[27] The as calculated average crystal sizes are 13.9 nm for Pt/$TiO_2$, and 22.4 nm for Pt/P25.

**3.1.2 SEM and STEM images** The shape and size of the nanoparticles are shown by SEM and STEM images. **Fig. 3 (a)** shows a representative SEM image of the $TiO_2$ nanoparticles calcined at 500 °C. The average $TiO_2$ nanoparticle size is 18.4 nm, while that for P25 is 27.5 nm. **Fig. 3 (b)** is a high-angle annular dark field (HAADF) STEM image of the Pt/$TiO_2$ nanoparticles. Ultrafine Pt with an average size of 1.82 nm (**Fig. 3 (c)**) is evenly distributed on the surface of $TiO_2$. A smaller particle size usually indicates a larger surface area. The BET surface area of Pt/$TiO_2$ (110.4 $m^2$/g) is much larger than that of Pt/P25 (59.7 $m^2$/g), and this is one of the reasons for the high photoactivity of Pt/$TiO_2$.

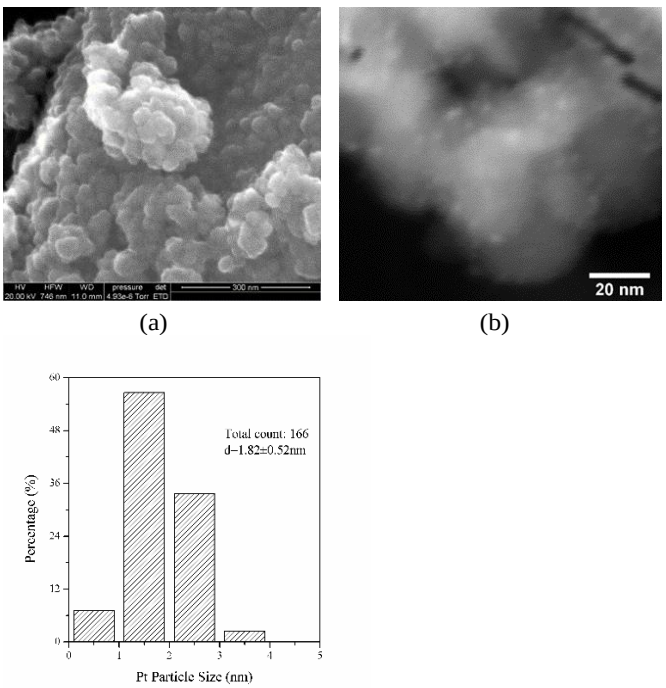


(a) (b)

(c)

**Fig. 3** (a) SEM image of $TiO_2$ (b) STEM image of Pt/$TiO_2$ (c) Pt particle size distribution for Pt/$TiO_2$

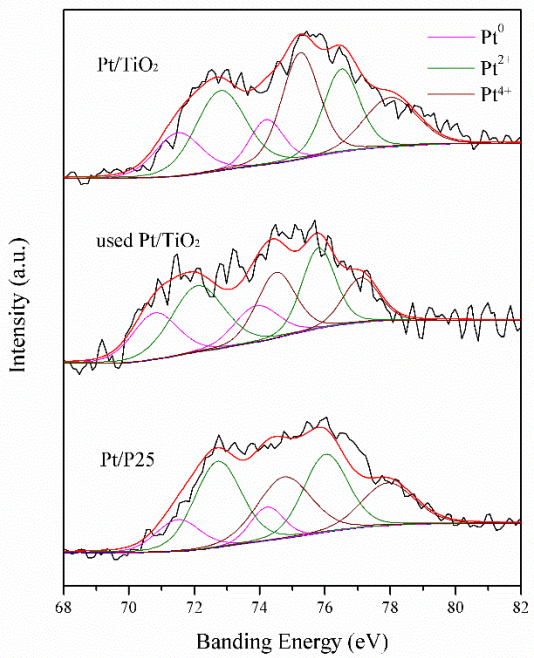


**Fig. 4** XPS spectra of Pt 4f level of $Pt/TiO_2$, used $Pt/TiO_2$ and Pt/P25

**3.1.3 XPS analysis** Compared with XRD, XPS is more sensitive for detection of surface species with low content. Hence, $Pt/TiO_2$ photocatalyst was investigated by XPS to verify the existence and oxidation states of Pt species. From **Fig. 4**, only part of the Pt species were fully reduced to metallic Pt. The most intense peaks at 71.3 eV and 74.4 eV are due to metallic Pt 4f core-level. The second set of doublets at 72.8 eV and 76.2 eV can be assigned to the photoemission of $Pt^{2+}$ chemical states such as PtO and $Pt(OH)_2$. The third doublets of Pt at higher binding energies of 74.8 eV and 78.0 eV are assigned to $Pt^{4+}$, such as $PtO_2$ or $Pt(OH)_4$.[28-30] The ratio of platinum species, $Pt^0/Pt^{2+}/Pt^{4+}$, was calculated with the peak areas of Pt $4f_{7/2}$. Compared to used $Pt/TiO_2$, the $Pt/TiO_2$ and Pt/P25 peaks have a positive shift. Such a positive shift is postulated for highly dispersed and small size Pt.[31] The negative shift from used $Pt/TiO_2$ may not only because of the Pt agglomeration, but also due to the fact that electrons transfer from $TiO_2$ to Pt because of a strong metal-support interaction (SMSI), which is based on the electronic and structural effects involving both the active metal and the support, and it may cause the rich electron states of Pt.[31, 32] The negative Pt would inhibit formation of Schottky barriers between P25 and metallic Pt, which increases the recombination of photo-induced electrons and holes and ultimately reduces the efficiency of $CO_2$ conversion.[33, 34] This is consistent with the fact that Pt nanoparticles grow bigger and partly explains the low efficiency of $CO_2$ conversion rate by used $Pt/TiO_2$.[35]

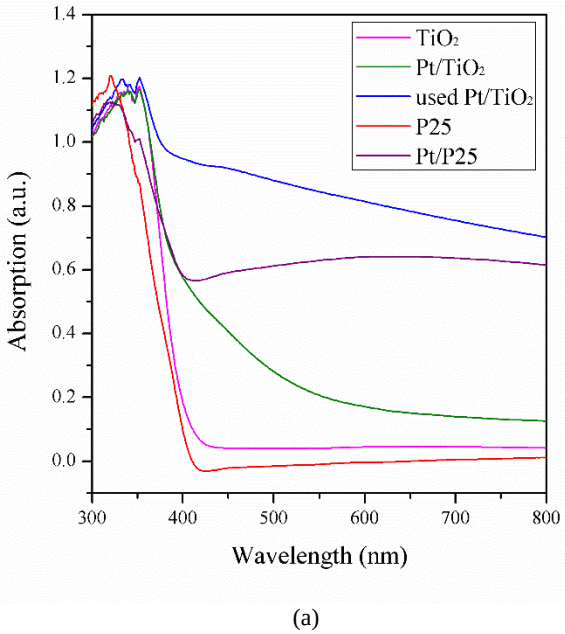


(a)

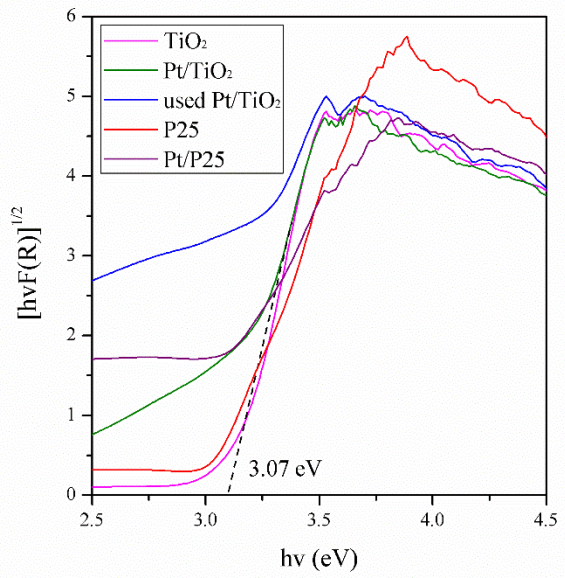


(b)

**Fig. 5** (a) UV-vis absorption spectra of $TiO_2$, $Pt/TiO_2$, used $Pt/TiO_2$, P25 and Pt/P25 (b) Corresponding plot of transformed Kubelka-Munk function versus the energy of the light

**3.1.4 UV-vis spectroscopy** The UV-vis light absorption is given in **Fig. 5 (a)**. The significant UV absorption below 390 nm is assigned to the intrinsic bandgap absorption of $TiO_2$ (~ 3.15 eV). The deposition of Pt on $TiO_2$ or P25 increases its visible light response ability.[25] Secondly, $PtO/Pt(OH)_2$ and $PtO_2/Pt(OH)_4$ on the surface also contribute to the visible light absorption.[36]

The corresponding diffuse-reflectance UV-vis spectra in **Fig. 5 (b)** were obtained according to the Kubelka-Munk function: $F(R)=(1-R)^2/2R$, in which R is the reflectance (%). The Kubelka-Munk function was then applied to the Tauc equation $(hvF(R))^{1/n}$ =

A(hv- Eg), where hv is the photo energy, Eg is the bandgap and A is a constant. For indirect allowed transition, n=2, since the fundamental absorption of $TiO_2$ possesses an indirect transition between bands. If $(hvF(R))^{1/2}$ is plotted against hv and a tangent line is drawn from the inflection point on the curve, the intersection of the tangent line with the horizontal axis is the bandgap.[37] As calculated, the bandgap of the $Pt/TiO_2$ is 3.07 eV.

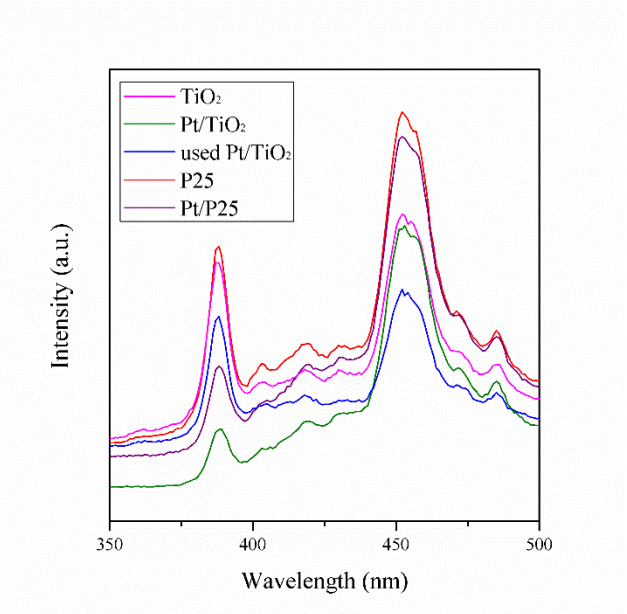


**Fig. 6** PL spectra of $TiO_2$, $Pt/TiO_2$, used $Pt/TiO_2$, P25 and Pt/P25

**3.1.5 PL spectroscopy** The PL emission results from the recombination of photogenerated electrons and holes, and a lower PL emission intensity usually indicates a decrease in radiative recombination and better separation of photogenerated electrons and holes.[38] To understand the efficiency of photogenerated charge transfer and separation of the $Pt/TiO_2$ photocatalyst, PL tests were carried out. **Fig. 6** presents a comparison of the PL spectra of several representative samples. For all the samples, two main emission peaks appear around 391 nm and 453 nm, which are equivalent to 3.17 and 2.74 eV, respectively. The 391 nm peak is due to the bandgap transition emission with the energy of emission light approximately equal to the bandgap energy of $TiO_2$.[34] The PL signals at about 430-500 nm mainly result from excitonic PL, due to surface oxygen vacancies and defects of the $TiO_2$ samples. The PL peak at 453 nm is attributed to band edge free excitons.[39] Two small peaks at 472 nm and 486 nm result from bound excitons.[40] As shown in **Fig. 6**, the $TiO_2$ bandgap emission is lower than P25, indicating the electron-hole recombination rate through radiative combination is lower than that of P25. The photodeposition of Pt nanoparticles generates considerable fluorescence quenching, which indicates the transfer of electrons from $TiO_2$ to Pt and the favorable contact between them. In addition, it should be noted that the PL peak of $Pt/TiO_2$ is weaker than that of Pt/P25, suggesting its lower electron-hole recombination rate through radiative combination. Under UV light irradiation, the electrons from the valence band of $TiO_2$ will be excited to the conduction band and then migrate rapidly to Pt nanoparticles, decreasing the direct recombination of charge carriers and finally contributing to the high photocatalytic performance.[25]

**Table 1** Characteristics of $Pt/TiO_2$ with $TiO_2$ calcined at different temperatures

| Samples | Structure[a] | Bandgap[b] (eV) | $TiO_2$ Particle Size[c] | Pt Particle Size[c] | Pt Weight Percentage[d] | $Pt^0$: $Pt^{4+}$ Ratio[d] | $Pt^{2+}$ | BET ($m^2/g$) |
|---|---|---|---|---|---|---|---|---|
| $Pt/TiO_2$-400 °C | anatase | 3.10 | 14.8±4.3 | 1.6±0.5 | 5.38‰ | 18:56:26 | | 128.5 |
| $Pt/TiO_2$-450 °C | anatase | 3.09 | 15.5±5.6 | 1.7±0.6 | 8.02‰ | 19:52:29 | | 124.6 |
| $Pt/TiO_2$-500 °C | anatase | 3.07 | 18.4±7.1 | 1.8±0.5 | 10.87‰ | 21:40:39 | | 110.4 |
| $Pt/TiO_2$-550 °C | anatase | 3.03 | 19.9±7.7 | 2.2±0.8 | 8.87‰ | 21:49:30 | | 49.7 |
| $Pt/TiO_2$-600 °C | anatase | 2.97 | 24.5±8.9 | 4.6±2.0 | 6.15‰ | 15:40:45 | | 37.7 |
| $Pt/TiO_2$-650 °C | anatase | 2.89 | 37.5±11.8 | N/A | 3.02‰ | N/A | | 12.1 |
| used $Pt/TiO_2$-500 °C | anatase | 2.83 | 18.4±7.1 | 1.9±0.7 | 10.63‰ | 26:43:31 | | 108.9 |

[a]Obtained by XRD [b]Calculated from UV-vis spectra [c]Measured from TEM images [d]Analyzed from ICP-OES

**3.1.6 Characteristics of $Pt/TiO_2$ with $TiO_2$ calcined at different temperatures** With the exception of the representative photocatalysts, the $Pt/TiO_2$ photocatalysts with $TiO_2$ calcined at different temperatures were also characterized. The results are shown in **Table 1**. It is obvious that with the increasing of calcination temperature, the $TiO_2$ particle size is increasing together with the decreasing of BET surface area. Meanwhile, with the same deposition time, the surface Pt atomic percentage first increased and then decreased with a further increasing calcination temperature from 500 °C. No metallic Pt was observed on $Pt/TiO_2$-650 °C, which agrees with **Fig. 8** that the photocatalytic activity decreased rapidly over this sample. While at 650 °C, the bandgap still decreased to 2.89 eV; this is probably due to the growing amount of $PtO/Pt(OH)_2$ and $PtO_2/Pt(OH)_4$ on the surface of $TiO_2$. After reaction, the surface Pt amount decreased, together with an increase in average Pt size (~ 1.98 nm), and this agrees with the experiment results of Bai et al.[41]

### 3.2 Factors affecting the performances of photocatalysts

**3.2.1 Preparation conditions of photocatalysts** $TiO_2$ calcined under different temperatures were used to synthesize $Pt/TiO_2$ and then used for photocatalytic $CO_2$ conversion. As shown in **Fig. 7**, with the increase in calcination temperature from 400 °C-500 °C, the photocatalytic $CO_2$ conversion ability kept increasing, and reached a maximum value at 500 °C. The $CH_4$ yield was 277.2 ppm [60.1μmol/($g_{cat}$·h)] after 4 h of illumination, together with a $H_2$ concentration of 389.2 ppm [87.5 μmol/($g_{cat}$·h)] and an $C_2H_6$ concentration of 12.4 ppm [2.8 μmol/($g_{cat}$·h)]. The increase in photoactivity is mainly due to the improved crystallization of anatase $TiO_2$, an appropriate surface Pt percentage (shown in **Table 1**), and an ultrafine Pt size (shown in **Fig. 3**). When the calcination temperature was higher than 550 °C, a sharp decrease in photoactivity was observed, which could be ascribed to bigger and agglomerated $TiO_2$,[42] a low Pt content and a decrease of $Pt^0$ state (shown in **Table 1**).

In addition to the effect of $TiO_2$ calcination temperature, the influence of Pt deposition time was investigated. **Fig. 8** shows the photocatalytic activity of P25, Pt/P25 and $Pt/TiO_2$ samples. Pure $TiO_2$ had a better photocatalytic activity than that of P25, with a $CH_4$ production of 12.4 ppm and a $H_2$ production of 68.3 ppm, while P25 could only produce 3.8 ppm $CH_4$, 11 ppm CO and 23.7 ppm $H_2$. The homemade $TiO_2$ preferentially produced $CH_4$, rather than CO, and had a higher photocatalytic water splitting ability. The Pt loading greatly promoted the photocatalytic activity of both $TiO_2$ and P25. As can be seen in **Fig. 8**, with the increase of Pt deposition time, the photocatalytic performance first sharply increased and then decreased slowly. The optimal photodeposition time was 1 h under the given experimental conditions. Considering that Pt was deposited on $TiO_2$ by photoreduction, the variation of the photocatalytic performance of $Pt/TiO_2$ might be due to different Pt nanoparticle content. With a short deposition time, not enough Pt was reduced. From ICP-OES test results, with a deposition time of 0.25 h, Pt counts for only 4.48‰ of the catalyst weight. It is accepted that Pt has a good ability to trap photogenerated electrons, but if not enough Pt was deposited, insufficient sites would not trap enough electrons

for $CO_2$ conversion.[43] The increase in photodeposition time improved the Pt content, promoting the photocatalytic activity. At the optimum Pt deposition time of 1 h, Pt weight percentage was 10.87‰ of the catalyst weight. At a Pt deposition time of 2 h, the Pt weight percentage was 13.92‰ of the catalyst weight. When the deposition time was beyond the optimum, too much Pt was deposited on the surface of $TiO_2$, which might block the light to the active sites on $TiO_2$ and retard the conversion of $CO_2$.[25, 44] For comparison, Pt/P25 was also prepared by the photodeposition method for 1 h under the same conditions. After photodeposition, the Pt weight percent was 11.21‰ of the catalyst weight, similar to that of $Pt/TiO_2$. The selectivity of P25 was changed after photodeposition. CO could not be detected. The production of $CH_4$ was 74 ppm [16.6 μmol/($g_{cat}$·h)] while $H_2$ was 151.4 ppm [34.0μmol/($g_{cat}$·h)], much smaller than that of $Pt/TiO_2$.

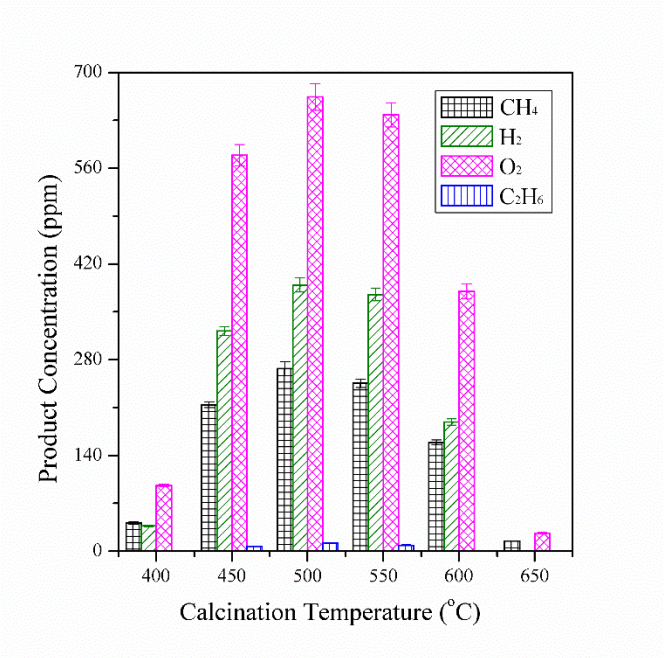


**Fig. 7** Effect of $TiO_2$ calcination temperature on the concentrations of products resulting from photocatalytic $CO_2$ conversion over $Pt/TiO_2$ (catalyst weight: 20 mg; water volume: 5 mL; $CO_2$ pressure: 4 bar; temperature: 80 °C)

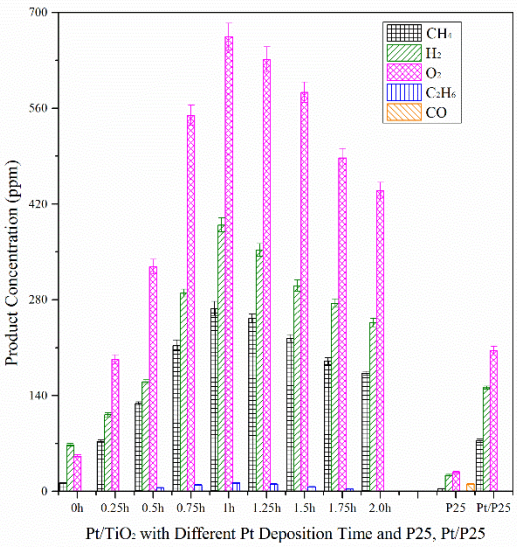


**Fig. 8** Comparison of photocatalytic performances of P25, Pt/P25 and $Pt/TiO_2$ with different Pt deposition time (catalyst weight: 20 mg; water volume: 5 mL; $CO_2$ pressure: 4 bar; temperature: 80 °C)

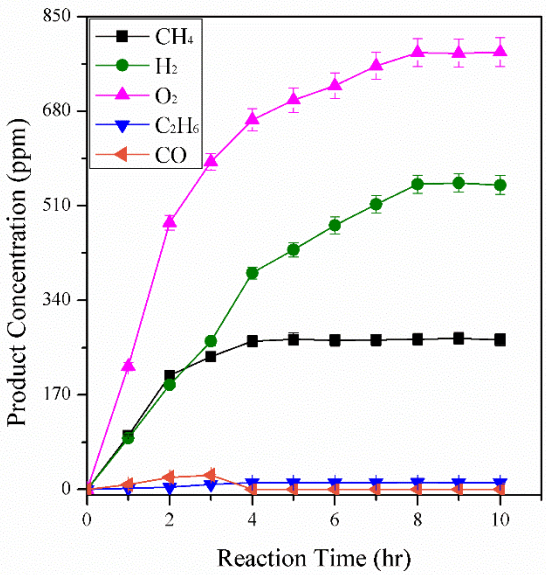


**Fig. 9** Effect of reaction time on the concentrations of products resulting from photocatalytic $CO_2$ conversion over $Pt/TiO_2$ (catalyst weight: 20 mg; water volume: 5 mL; $CO_2$ pressure: 4 bar; temperature: 80 °C)

**3.2.2 Effects of reaction conditions** In addition to the photocatalyst itself, the reaction conditions also show great effect on the photocatalytic reaction. Hence, the influence of reaction time, reaction temperature and $CO_2$ concentration on the photocatalytic performance of the optimized $Pt/TiO_2$ samples were investigated. **Fig. 9** is a plot of the product concentration under different reaction time. The products include $CH_4$, CO, $H_2$, $C_2H_6$ and $O_2$. As can be

seen in **Fig. 9**, for the first 4 h, $CH_4$ concentration kept increasing and reached a peak of 277.2 ppm. Under longer irradiation, the concentration of $CH_4$ did not grow anymore, which might be due to the deterioration of the photocatalyst, resulting from the saturation of adsorption sites on the $Pt/TiO_2$ surface with intermediate products.[45] This can be proved by repeated use of $Pt/TiO_2$ photocatalysts. After removing the intermediate products, $Pt/TiO_2$ photocatalyst still had 88.6% of its original activity. In the first 3 h CO was detected with a peak concentration of 25.9 ppm, and then it disappeared. After longer reaction time, CO diminished when more photogenerated electrons were created; this phenomenon can be attributed to the further conversion of CO to $CH_4$, since $CH_4$ formation is an 8-electron photoreduction process, while the formation of CO only needs 2 electrons.[46] The diminishment of CO can also be explained by the electrochemical potential, -0.53V/NHE (normal hydrogen electrode) for CO and -0.24V/NHE for $CH_4$, which indicates that $CH_4$ is more stable than CO.[26] In addition to $CH_4$ and CO, $C_2H_6$ was detected and reached its highest concentration (12.3 ppm) at 4 h. This value remained unchanged at longer irradiation. The generation of $C_2H_6$ occurs when the system has an abundance of photogenerated electrons, and can't provide enough •H for $•CH_3$, since •H has participated in $H_2$ production.[47] Output of $H_2$ kept increasing during 8 h of irradiation, reaching 548.8 ppm. This demonstrated the photocatalytic water splitting ability of $Pt/TiO_2$ to form •H, which is in accordance with the report of Nada, in which $H_2O$ is an electron acceptor and competes with $CO_2$ to accept electrons.[45] The high $H_2$ yield may be partly due to enough water coverage on the catalyst surface, which contributes to the generation of •H and the transport of •H to $CO_2$.[48] The different increases of $CH_4$ and $H_2$ demonstrate a difference in the intermediate balance concentration and further different reaction active sites.[42] Along with the reduction products, $O_2$ was detected in our system. After reaction, the liquid was carefully analyzed by Agilent 1260 Infinity HPLC and Agilent 5975 C GC-MS, but potential products such as $CH_3OH$, $CH_2OH$ and HCOOH were not detected.

Control experiments were carried out to rule out possibilities of carbon contamination during the preparation process, such as incomplete reaction of titanium n-butoxide, or from $CH_3OH$ during Pt photodeposition. When He (5.0 UHP, 99.999%) was used as the carrier gas instead of introducing $CO_2$ into the reactor, while all the other condition remained the same, no $CH_4/C_2H_6$ was detected, suggesting that all the $CH_4$ and $C_2H_6$ came from $CO_2$ conversion. Also, without light illumination, no product was detected, demonstrating light illumination is the driving force and $CO_2$ conversion is a photocatalytic process.

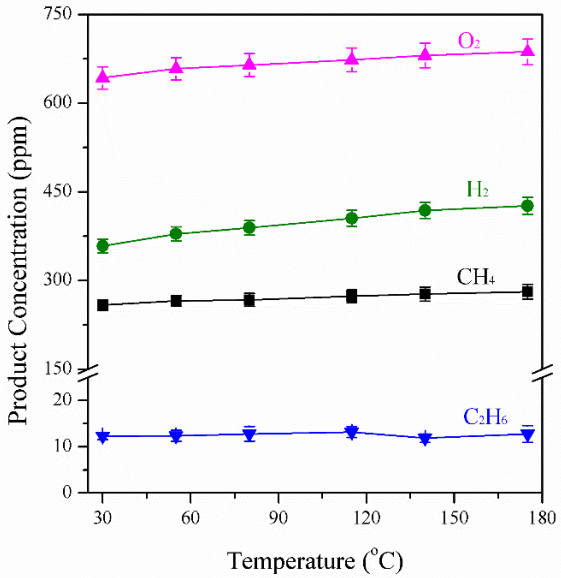


**Fig. 10** Effect of temperature on the concentrations of products resulting from photocatalytic $CO_2$ conversion over $Pt/TiO_2$ (catalyst weight: 20 mg; water volume: 5 mL; $CO_2$ pressure: 4 bar)

**Fig. 10** shows the effect of reaction temperature on the photocatalytic performance of $Pt/TiO_2$. It is known that the photocatalytic efficiency mainly depends on the photogenerated electron-hole pair separation and reaction, but a higher temperature can increase the diffusion rate and collision frequency.[4] As shown in **Fig. 10**, the concentration of $C_2H_6$ increased slightly with an increase in temperature, while $CH_4$ output increased 8.7%, with a concentration change from 258.4 ppm at 30 °C to 280.9 ppm at 175 °C. Output of $H_2$ increased 19.0%, with a concentration change from 358.4 ppm at 30 °C to 426.5 ppm at 175 °C. The increased temperature speeded up the desorption process during the heterogeneous photocatalytic reaction, resulting in a higher reaction rate.[49] Hence, the output of products was increased. Meanwhile, it can be noticed that the reaction temperature had a stronger influence on $H_2$ production than on $CH_4$. This phenomenon may be attributed to an improved concentration of water vapor with the increased temperature, which is beneficial for water splitting.

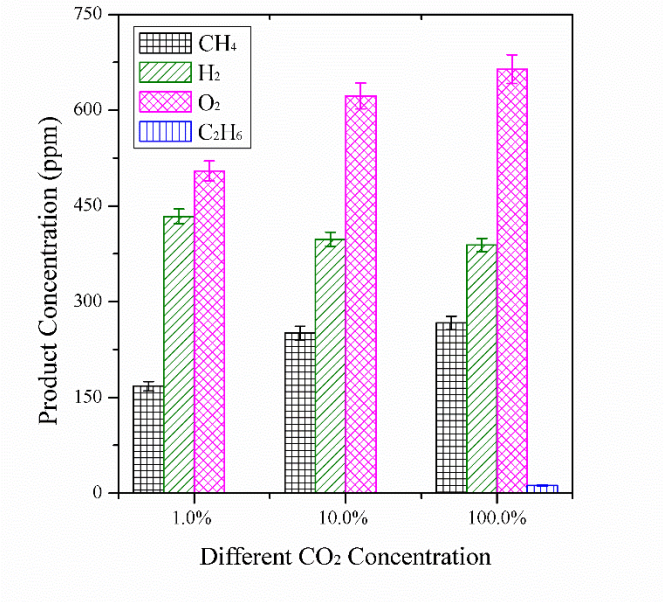


**Fig. 11** Effect of $CO_2$ concentration on the concentrations of products resulting from photocatalytic $CO_2$ conversion over $Pt/TiO_2$ (catalyst weight: 20 mg; water volume: 5 mL; total pressure: 4 bar; temperature: 80 $^oC$)

In addition to the effects of reaction time and temperature, the influence of $CO_2$ concentration on the photoactivity was also investigated. For these tests, 1.0% and 10.0% concentration of $CO_2$ diluted with $N_2$ were used. From **Fig. 11**, the $CH_4$ production of 1.0% $CO_2$ was 167.9 ppm, accounting for 60.8% of the $CH_4$ yield of pure $CO_2$. For the 10.0% $CO_2$, the $CH_4$ production was 251 ppm, accounting for 90.5% of the $CH_4$ yield of pure $CO_2$ and demonstrating the potential ability to photocatalytically convert flue gas into $CH_4$. As can be seen, the $H_2$ production with diluted $CO_2$ was even higher than the $H_2$ production with pure $CO_2$, which may be because there was more •H bonded to form $H_2$, instead of reacting with $•CH_3$, due to the decreased $CO_2$ content.[50] No $C_2H_6$ was observed with diluted $CO_2$ since there was enough •H and all $•CH_3$ bonded with •H instead of $•CH_3$.

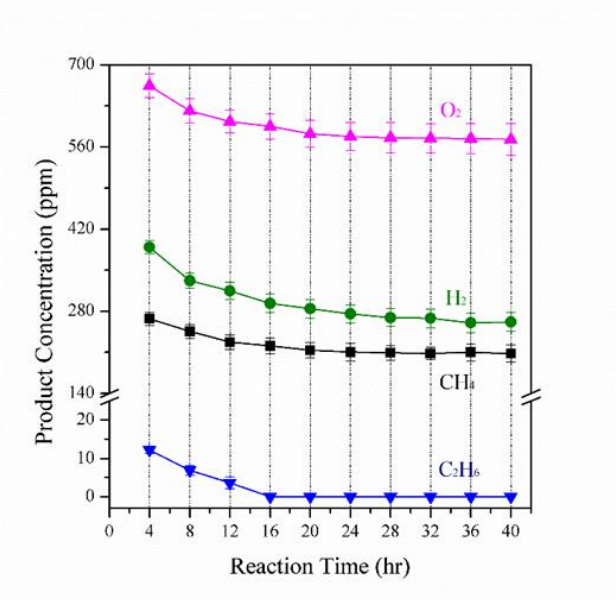


**Fig. 12** Time course of photocatalytic $CO_2$ conversion over $Pt/TiO_2$ (catalyst weight: 20 mg; water volume: 5 mL; $CO_2$ pressure: 4 bar; temperature: 80 $^oC$)

### 3.3 Photocatalyst stability

Although $Pt/TiO_2$ photocatalyst demonstrates high photocatalytic performance in $CO_2$ conversion, its stability is still very important for practical applications. Repeated uses of $Pt/TiO_2$ on photocatalytic $CO_2$ conversion were conducted to explore the $Pt/TiO_2$ stability. These experiments were tested every 4 h for ten times. Each time, after one round, the reacted gas was evacuated and new $CO_2$ and DI water were introduced. As can be seen in **Fig. 12**, after one cycle, the $CH_4$ output dropped to 245.6 ppm, accounting for 88.6% of its original photocatalytic ability, while the $H_2$ output decreased from 389.2 ppm to 332.1 ppm. Subsequently, $Pt/TiO_2$ gradually became stable and the $CH_4$ evolution didn't change after five rounds of reaction. After three rounds of reaction, there was no $C_2H_6$ produced, due to the deterioration of photocatalysts. After 10 rounds of reaction, the $CH_4$ concentration was 207.9 ppm and the $H_2$ was 257.8 ppm, demonstrating 75.8% of the original $CH_4$ output; this was still 2.8 times that of Pt/P25. In comparison, the $CH_4$ concentration over Pt/P25 dropped to 60.2 ppm only after one cycle, accounting for 81.4% of its original photocatalytic ability and was lower than that of $Pt/TiO_2$.

**Table 2** Calculated $O_2$ concentration *vs.* measured $O_2$ concentration

| Time (h) | $O_{2,m}$ (ppm) | $O_{2,c}$ (ppm) | Error[a] (%) |
|---|---|---|---|
| 1 | 221.2 | 252.8 | 12.50f |
| 2 | 479.7 | 529.75 | 9.45 |
| 3 | 589.1 | 656.35 | 10.25 |
| 4 | 664.4 | 783.4 | 15.19 |
| 5 | 699.6 | 798.15 | 12.35 |
| 6 | 725.7 | 815.95 | 11.06 |
| 7 | 761.4 | 837.15 | 9.05 |
| 8 | 785.3 | 859.2 | 8.60 |

[a]Error was calculated by $(O_{2,c} - O_{2,m})/O_{2,c}$

### 3.4 Reaction mechanism

The generation of electron-hole pairs upon UV irradiation and the migration of the charges on $Pt/TiO_2$ photocatalyst are obvious. The photoexcited electrons generated by $TiO_2$ are trapped by the Pt nanoparticles and the surface reduction process takes place on Pt nanoparticles, while the holes stay on $TiO_2$ to oxidize $H_2O$ to $O_2$. However, the photocatalytic $CO_2$ conversion process is not clear. Based on previous literature and the data obtained in this research, photocatalytic $CO_2$ conversion might occur according to the following process: $CO_2$ is first reduced to CO at the Pt sites, while at the same time •H is formed from water splitting. Then the as-formed CO reacts with •H to form $CH_4$ and $C_2H_6$.[46, 51] Formation of $O_2$ was detected. For example, over the $Pt/TiO_2$ catalyst and a reaction time of 4 h, the $O_2$ concentration reached 664.4 ppm, the $CH_4$ concentration reached 277.2 ppm, together with a $H_2$ concentration of 389.2 ppm and an $C_2H_6$ concentration of 12.4 ppm. From the concentration of the reductive products, the stoichiometric formation of $O_2$ was calculated by assuming that the oxidation of water to form $O_2$ is the only source to provide electrons. The $O_2$ calculated concentration ($O_{2,c}$), based on the

quantities of measured $H_2$, $CH_4$, and $C_2H_6$, can be estimated as follows :

$O_{2,c} = 0.5H_{2,m} + 0.5CO_m + 2CH_{4,m} + 3.5\ C_2H_{6,m}$

where $H_{2,m}$, $CO_m$, $CH_{4,m}$ and $C_2H_{6,m}$ refer to the measured concentration of $H_2$, CO, $CH_4$ and $C_2H_6$, respectively. The calculated $O_2$ concentration and the measured $O_2$ formation concentration ($O_{2,m}$) under different reaction time are listed in **Table 2**. The errors between them are listed. Considering the actual $O_2$ formation is similar to the calculated stoichiometric $O_2$ formation value, the following reaction pathways at pH=7 are proposed:[19, 26]

$TiO_2 + h\nu \rightarrow TiO_2^* (e^- + h^+)$

Valance band (photooxidation)

$2H_2O+4h^+ \rightarrow 4H^+ + O_2$; $E^o_{redox}$= 0.82 V vs NHE

Conduction band (electrons transfer)

$TiO_2 (e^-,CB) + Pt \rightarrow TiO_2 (CB) + Pt (e^-)$

Pt surface (photoreduction)

$2H^+ + 2e^- \rightarrow H_2$; $E^o_{redox}$= -0.42 V vs NHE

$CO_2+2H^++2e^- \rightarrow CO+H_2O$; $E^o_{redox}$ = -0.53 V vs NHE

$CO_2+8H^++8e^- \rightarrow CH_4+2H_2O$; $E^o_{redox}$ = -0.24 V vs NHE

$2CO_2+14H^++14e^- \rightarrow C_2H_6+4H_2O$; $E^o_{redox}$ = -0.27 V vs NHE

## 4. Conclusions

In summary, well-crystallized anatase $TiO_2$ nanoparticles with a high surface area and a diameter of ~ 18.4 nm were prepared by a solvothermal method at 180 °C. $Pt/TiO_2$ nanocomposites with an average Pt nanoparticle size of 1.82 nm were then prepared by photoreduction and used for photocatalytic $CO_2$ conversion. XPS analysis indicated that only part of the Pt species were reduced to metallic Pt. The $Pt/TiO_2$ nanocomposites had a bandgap of 3.07 eV, and the photogenerated electron-hole recombination rate was lower than that of Pt/P25. Pt photodeposition time and $TiO_2$ calcination temperature had a significant impact on the photoactivity of $Pt/TiO_2$, and the optimal $TiO_2$ calcination temperature and Pt photodeposition time were 500 °C and 1 h, respectively. The optimized $Pt/TiO_2$ presented a photoactivity 3.7 times higher than that of Pt/P25 and 18.7 times higher than that of P25. Reaction temperature had a slight influence on the photocatalytic $CO_2$ conversion process. By using 10.0% $CO_2$ diluted in $N_2$, the $CH_4$ yield was 90.5% that of pure $CO_2$. Moreover, The $Pt/TiO_2$ nanocomposites were more stable than Pt/P25 and could be used repeatedly. In addition, $O_2$ was detected and recorded for a systematic analysis of the relationship between photocatalytic $CO_2$ conversion and water splitting, and the balance between the photogenerated electrons and holes were calculated. It is proposed that CO and •H were formed at first and then the as-formed CO reacted with •H to form $CH_4$ and $C_2H_6$.

## Acknowledgements

The authors greatly appreciate the supports from the Clean Coal Program and School of Energy Resources in Wyoming, and the Department of Energy in the US, as well as Nanjing University of Technology in China.

## Notes and references

[a] Department of Chemical & Petroleum Engineering, University of Wyoming, Laramie, WY, 82071, USA

[b] School of Chemical and Environmental Engineering, China University of Mining and Technology, Beijing 100083, China

[c] College of Materials Science and Engineering, Nanjing University of Technology, Nanjing, 210009, China

[d] School of Energy Resources, University of Wyoming, Laramie, WY, 82071, USA

[e] Department of Materials Physics, Zhejiang Normal University, Jinhua, 321004, China

[f] Department of Chemistry, University of Kansas, Lawrence, KS, 66045, USA

1. S. Cui, W. Cheng, X. Shen, M. Fan, A. T. Russell, Z. Wu, X. Yi, *Energy & Environmental Science*, 2011, **4**, 2070.
2. B. Dutcher, M. Fan, B. Leonard, M. D. Dyar, J. Tang, E. A. Speicher, P. Liu, Y. Zhang, *The Journal of Physical Chemistry C*, 2011, **115**, 15532.
3. B. T. Zhang, M. Fan, A. E. Bland, *Energy & Fuels*, 2011, **25**, 1919.
4. P. Usubharatana, D. McMartin, A. Veawab, P. Tontiwachwuthikul, *Industrial & Engineering Chemistry Research*, 2006, **45**, 2558.
5. L. Cao, S. Sahu, P. Anilkumar, C. E. Bunker, J. Xu, K. S. Fernando, P. Wang, E. A. Guliants, K. N. Tackett, Y. P. Sun, *Journal of the American Chemical Society*, 2011, **133**, 4754.
6. D. Ravelli, D. Dondi, M. Fagnoni, A. Albini, *Chemical Society Reviews*, 2009, **38**, 1999.
7. S. Kwon, M. Fan, A. T. Cooper, H. Yang, *Critical Reviews in Environmental Science and Technology*, 2008, **38**, 197.
8. O. K. Varghese, M. Paulose, T. J. LaTempa, C. A. Grimes, *Nano Letters*, 2009, **9**, 731.
9. M. Halmann, *Nature*, 1978, **275**, 115.
10. W. Fan, Q. Zhang, Y. Wang, *Physical Chemistry Chemical Physics*, 2013, **15**, 2632.
11. Q. Liu, Y. Zhou, J. Kou, X. Chen, Z. Tian, J. Gao, S. Yan, Z. Zou, *Journal of the American Chemical Society*, 2010, **132**, 14385.
12. H. Huang, D. Li, Q. Lin, W. Zhang, Y. Shao, Y. Chen, M. Sun, X. Fu, *Environmental Science & Technology*, 2009, **43**, 4164.
13. W. Tu, Y. Zhou, Q. Liu, Z. Tian, J. Gao, X. Chen, H. Zhang, J. Liu, Z. Zou, *Advanced Functional Materials*, 2012, **22**, 1215.
14. L. Luo, A. T. Cooper, M. Fan, *Journal of Hazardous Materials*, 2009, **161**, 175.
15. X. Chen, S. S. Mao, *Chemical Reviews*, 2007, **107**, 2891.
16. H. Tada, T. Kiyonaga, S. I. Naya, *Chemical Society Reviews*, 2009, **38**, 1849.
17. Y. Xie, K. Ding, Z. Liu, R. Tao, Z. Sun, H. Zhang, G. An, *Journal of the American Chemical Society*, 2009, **131**, 6648.
18. Q. H. Zhang, W. D. Han, Y. J. Hong, J. G. Yu, *Catalysis Today*, 2009, **148**, 335.
19. Q. Zhai, S. Xie, W. Fan, Q. Zhang, Y. Wang, W. Deng, Y. Wang, *Angewandte Chemie*, 2013, **125**, 5888.
20. J. Liao, L. Shi, S. Yuan, Y. Zhao, J. Fang, *The Journal of Physical Chemistry C*, 2009, **113**, 18778.
21. C. Hu, X. Zhang, W. Li, Y. Yan, G. Xi, H. Yang, J. Li, H. Bai, *Journal of Materials Chemistry A*, 2014, **2**, 2040.
22. G. Li, S. Ciston, Z. V. Saponjic, L. Chen, N. M. Dimitrijevic, T. Rajh, K. A. Gray, *Journal of Catalysis*, 2008, **253**, 105.

23. S. Lee, I. S. Cho, J. H. Lee, D. H. Kim, D. W. Kim, J. Y. Kim, H. Shin, J. K. Lee, H. S. Jung, N. G. Park, *Chemistry of Materials*, 2010, **22**, 1958.
24. Y. Jiao, C. Peng, F. Guo, Z. Bao, J. Yang, L. Schmidt-Mende, R. Dunbar, Y. Qin, Z. Deng, *The Journal of Physical Chemistry C*, 2011, **115**, 6405.
25. J. Yu, L. Qi, M. Jaroniec, *The Journal of Physical Chemistry C*, 2010, **114**, 13118.
26. W. N. Wang, W. J. An, B. Ramalingam, S. Mukherjee, D. M. Niedzwiedzki, S. Gangopadhyay, P. Biswas, *Journal of the American Chemical Society*, 2012, **134**, 11276.
27. C. Chen, P. Liu, C. Lu, *Chemical Engineering Journal*, 2008, **144**, 509.
28. J. Wang, G. Yin, Y. Shao, S. Zhang, Z. Wang, Y. Gao, *Journal of Power sources*, 2007, **171**, 331.
29. R. E. Rettew, N. K. Allam, F. M. Alamgir, *ACS Applied Materials & Interfaces*, 2011, **3**, 147.
30. J. Lee, W. Choi, *The Journal of Physical Chemistry B*, 2005, **109**, 7399.
31. O. S. Alexeev, S. Y. Chin, M. H. Engelhard, L. Ortiz-Soto, M. D. Amiridis, *The Journal of Physical Chemistry B*, 2005, **109**, 23430.
32. A. Lewera, L. Timperman, A. Roguska, N. Alonso-Vante, *The Journal of Physical Chemistry C*, 2011, **115**, 20153.
33. F. Zhao, Y. Ikushima, M. Shirai, T. Ebina, M. Arai, *Journal of Molecular Catalysis A: Chemical*, 2002, **180**, 259.
34. L. Nie, J. Yu, X. Li, B. Cheng, G. Liu, M. Jaroniec, *Environmental Science & Technology*, 2013, **47**, 2777.
35. W. Kong, B. Tian, J. Zhang, D. He, M. Anpo, *Research on Chemical Intermediates*, 2013, **39**, 1701.
36. F. Li, X. Li, *Chemosphere*, 2002, **48**, 1103.
37. W. Fan, Q. Lai, Q. Zhang, Y. Wang, *The Journal of Physical Chemistry C*, 2011, **115**, 10694.
38. J. Shi, J. Chen, Z. Feng, T. Chen, Y. Lian, X. Wang, C. Li, *The Journal of Physical Chemistry C*, 2007, **111**, 693.
39. N. Wu, J. Wang, D. N. Tafen, H. Wang, J. G. Zheng, J. P. Lewis, X. Liu, S. S. Leonard, A. Manivannan, *Journal of the American Chemical Society*, 2010, **132**, 6679.
40. M. Zhou, J. Yu, S. Liu, P. Zhai, L. Jiang, *Journal of Hazardous Materials*, 2008, **154**, 1141.
41. Y. Bai, W. Li, C. Liu, Z. Yang, X. Feng, X. Lu, K. Y. Chan, *Journal of Materials Chemistry*, 2009, **19**, 7055.
42. G. Li, N. M. Dimitrijevic, L. Chen, J. M. Nichols, T. Rajh, K. A. Gray, *Journal of the American Chemical Society*, 2008, **130**, 5402.
43. T. Chen, Z. Feng, G. Wu, J. Shi, G. Ma, P. Ying, C. Li, *The Journal of Physical Chemistry C*, 2007, **111**, 8005.
44. M. Huang, C. Xu, Z. Wu, Y. Huang, J. Lin, J. Wu, *Dyes and Pigments*, 2008, **77**, 327.f
45. N. M. Dimitrijevic, B. K. Vijayan, O. G. Poluektov, T. Rajh, K. A. Gray, H. He, P. Zapol, *Journal of the American Chemical Society*, 2011, **133**, 3964.
46. Y. Li, W. N. Wang, Z. Zhan, M. H. Woo, C. Y. Wu, P. Biswas, *Applied Catalysis B: Environmental*, 2010, **100**, 386.
47. W. Tu, Y. Zhou, Q. Liu, S. Yan, S. Bao, X. Wang, M. Xiao, Z. Zou, *Advanced Functional Materials*, 2013, **23**, 1743.
48. G. Ketteler, S. Yamamoto, H. Bluhm, K. Andersson, D. E. Starr, D. F. Ogletree, H. Ogasawara, A. Nilsson, M. Salmeron, *The Journal of Physical Chemistry C*, 2007, **111**, 8278.
49. M. Tahir, N. S. Amin, *Applied Catalysis B: Environmental*, 2013, **142**, 512.
50. G. Dey, *Journal of Natural Gas Chemistry*, 2007, **16**, 217.
51. X. Feng, J. D. Sloppy, T. J. LaTempa, M. Paulose, S. Komarneni, N. Bao, C. A. Grimes, *Journal of Materials Chemistry*, 2011, **21**, 13429.



 